Volume 6
Number 16
21 August 2024
Pages 3981–4262

Nanoscale Advances

rsc.li/nanoscale-advances

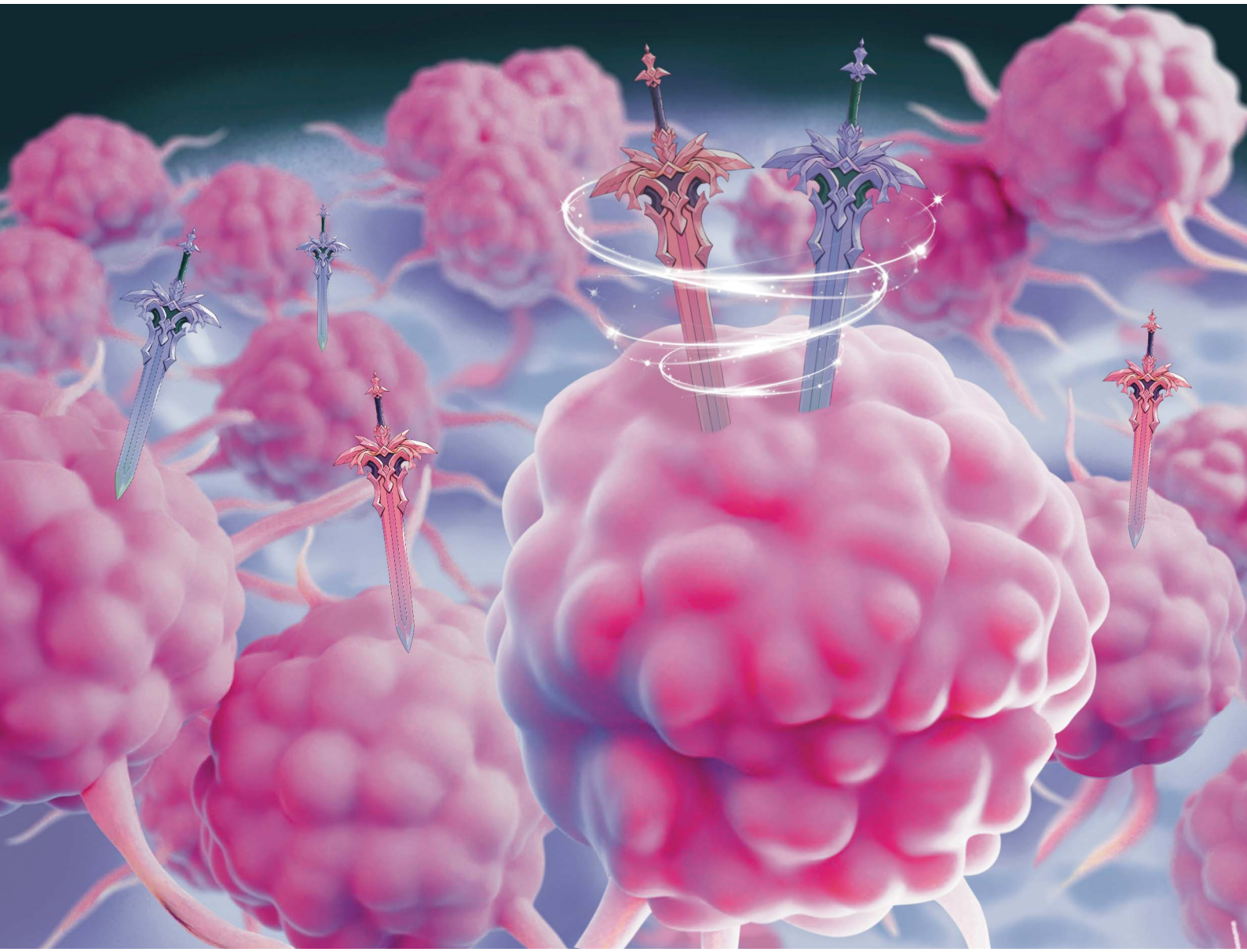

ISSN 2516-0230

ROYAL SOCIETY OF CHEMISTRY

PAPER

Ning Zhang, Lan Dai, Wen Di *et al.*
Nanoparticle co-delivery of carboplatin and PF543 restores platinum sensitivity in ovarian cancer models through inhibiting platinum-induced pro-survival pathway activation

NCNST

Nanoscale Advances

ROYAL SOCIETY OF CHEMISTRY

PAPER

View Article Online
View Journal | View Issue

Cite this: *Nanoscale Adv.*, 2024, **6**, 4082

Nanoparticle co-delivery of carboplatin and PF543 restores platinum sensitivity in ovarian cancer models through inhibiting platinum-induced pro-survival pathway activation†

Chen Wang,‡[ab] Qing Li,‡[ab] Keqi Song,[ab] Wenjing Wang,[ab] Ning Zhang,*[ab] Lan Dai *[ab] and Wen Di*[abc]

Resistance to platinum-based chemotherapy is the major cause of poor prognosis and cancer-associated mortality in ovarian cancer patients, so novel therapeutic strategies to restore platinum sensitivity are needed to improve patient outcomes. Sphingosine Kinase (SphK) 1 is involved in regulating multiple pro-survival pathways, key mediators in the sensitivity of tumor cells toward platinum. By encapsulating CBP and the SphK1 inhibitor PF543 in PLGA (poly lactic-*co*-glycolic acid) nanoparticles, a dual-drug delivery system (C/PNPs) was formed to simultaneously deliver CBP and PF543. The physicochemical characteristics, cell uptake rate and biodistribution behavior of C/PNPs were evaluated. Then the anti-tumor ability of C/PNPs *in vitro* and *in vivo* was further investigated. The C/PNPs could deliver CBP and PF543 simultaneously to a platinum-insensitive cell line (SKOV3) both *in vitro* and *in vivo*. Furthermore, benefiting from the enhanced permeability and retention (EPR) effect of PLGA NPs, C/PNPs exhibited an improved tumor region accumulation. As a result, a synergistic anti-tumor effect was found in the SKOV3 tumor-bearing mice, with tumor volume inhibiting rates of 84.64% and no side effects in major organs. The mechanistic studies confirmed that the inhibition of SphK1 by PF543 sensitized SKOV3 cells to CBP chemotherapy, partly by inhibiting the CBP-induced activation of pro-survival pathways, including ERK, AKT and STAT3 signaling. Our study reveals that C/PNPs can serve as an efficient dual-drug delivery system to restore platinum sensitivity in ovarian cancer models partly through inhibiting platinum-induced pro-survival pathway activation.

Received 19th March 2024
Accepted 29th May 2024

DOI: 10.1039/d4na00227j

rsc.li/nanoscale-advances

1 Introduction

Ovarian cancer is the leading cause of death from gynecological malignancy, with approximately 12 810 deaths and nearly 19 880 new cases estimated for 2022 in the United States.[1] Debulking surgery combined with platinum-based chemotherapy is the current first-line treatment for ovarian cancer.[2] Although initial ovarian cancer response rates to platinum-based chemotherapy are high, most of the ovarian cancer patients developed resistance to platinum during the period of treatment,[3] which is the major cause of poor prognosis[4] and ovarian cancer-associated mortality. Thus, novel therapeutic strategies to restore platinum sensitivity are needed to improve patient outcomes.

Extensive published evidence has demonstrated that platinum resistance stems from three primary mechanisms: (1) increased drug efflux and/or reduced drug uptake, (2) enhanced DNA repair and (3) upregulation of anti-apoptotic factors.[5,6] Pro-survival pathways are reported to play critical roles in the sensitivity of tumor cells toward platinum through these mechanisms. For example, signal transducer and activator of transcription 3 (STAT3), extracellular signal-regulated kinase (ERK) or protein kinase B (PKB/AKT) pathway activation can mediate the alterations of molecules involved in apoptosis, assist ovarian cancer cells to evade death, and ultimately cause the platinum-resistance of ovarian cancer.[7] Moreover, the AKT pathway could promote CDDP efflux and resistance by up-regulating drug transporters.[8] Accordingly, co-interfering with these specific pro-survival pathways may emerge as a promising strategy for overcoming platinum resistance. Therefore, we wondered whether there might be one major mediator regulating these signaling pathways.

[a]*Department of Obstetrics and Gynecology, Ren Ji Hospital, School of Medicine, Shanghai Jiao Tong University, Shanghai 200127, China. E-mail: ningning1723@126.com; delta496@163.com; diwen163@163.com*

[b]*Shanghai Key Laboratory of Gynecologic Oncology, Ren Ji Hospital, School of Medicine, Shanghai Jiao Tong University, Shanghai 200127, China*

[c]*State Key Laboratory of Oncogenes and Related Genes, Shanghai Cancer Institute, Ren Ji Hospital, School of Medicine, Shanghai Jiao Tong University, Shanghai 200127, China*

† Electronic supplementary information (ESI) available. See DOI: https://doi.org/10.1039/d4na00227j

‡ Chen Wang and Qing Li have contributed equally to this work.

PF543, a sphingosine kinase (SphK) 1 inhibitor, might be a suitable candidate drug because SphK1 plays important roles in regulating pro-survival pathways in cancer. SphK1 is an important signaling enzyme that could catalyze the phosphorylation of sphingosine and sequentially yield abundant sphingosine-1-phosphate (S1P).[9] It is well known that SphK1 could promote cell growth, inhibit apoptosis, and facilitate oncogenesis.[10] Researchers have found that the expression of SphK1 was up regulated in many solid tumors.[11] And the down-regulation of SphK1 by inhibitors or genetic means could be used as a novel way to suppress the growth of tumor.[12] Our previous studies have revealed that SphK1 mediated AKT and ERK pathways in ovarian cancer models.[13] Moreover, SphK1 was reported to regulate the STAT3 pathway and promote the development of colitis-associated cancer, bladder cancer and non-small cell lung cancer.[14–16] Importantly, previously we found that the expression level of SphK1 was higher in ovarian cancer cells and even higher in platinum-insensitive ovarian cancer cells, compared with the expression in normal controls,[17] which suggested that SphK1 may be involved in the platinum resistance of ovarian cancer. Based on these findings, we hypothesized that the combination of platinum drugs and PF543 may restore platinum sensitivity in ovarian cancer models.

Each chemotherapy drug or combination has nonspecific or systemic side effects, such as acute nephrotoxicity and adverse gastrointestinal reactions. As a solution, our previous studies showed that poly lactic-*co*-glycolic acid (PLGA) based nanoparticles (NPs) reduced these adverse effects, achieved sustained release and had good safety.[18,19] In recent years, PLGA-based nanoparticles (NPs) have been studied in the field of drug delivery, including the delivery of various anticancer drugs, protein or peptide drugs, and bacterial or viral DNA.[20,21] Therefore, PLGA NPs are particularly attractive for clinical application as drug delivery systems.

Based on the above scientific background, we investigated the role of PLGA nanoparticle co-delivery of carboplatin (CBP) and PF543 in restoring platinum sensitivity in platinum-insensitive ovarian cancer models. Owing to the enhanced permeability and retention (EPR) effect, C/PNPs showed an improved tumor preferential accumulation and cellular uptake rate. Moreover, mechanistic studies showed that PF543, an SphK1 inhibitor, significantly inhibited the CBP-induced activation of pro-survival pathways, including ERK, AKT and STAT3 pathways. As a result, synergistic anticancer effects were achieved both *in vitro* and *in vivo* (Scheme 1).

2 Materials and methods

2.1. Materials

PLGA (50 : 50) was obtained from Ruixi Biological Technology (Xi'an, China). Coumarin-6 and DiR iodide were purchased from MedChemExpress (Monmouth Junction, NJ, USA). CBP and PF543 were obtained from Sigma-Aldrich. Antibodies targeting SphK1 (catalog: 12071, rabbit), ERK (catalog: 4695, rabbit), p-ERK (catalog: 4370, rabbit), AKT (catalog: 4691, rabbit), p-AKT (catalog: 4060, rabbit), STAT3 (catalog: 4904, rabbit), p-STAT3 (catalog: 9145, rabbit) and GAPDH (catalog: 97166, mouse) were bought from Cell Signaling Technology (Danvers, MA, USA). Antibody targeting p-SphK1 (catalog: SP1641, rabbit) was purchased from ECM Biosciences.

2.2. Cell culture

The human ovarian cancer cell line SKOV3, which is insensitive to platinum,[22,23] was purchased from the Cell Bank of Type Culture Collection of the Chinese Academy of Sciences (Shanghai, China). The cells were cultured in DMEM medium supplemented with 10% FBS and 1% penicillin–streptomycin at 37 °C in 5% CO_2.

2.3. Synthesis and characterization of C/PNPs

C/PNPs were formulated by the double emulsion technique.[24] We tested the encapsulation efficiency of different ratios of PF543 and CBP ranging from 5 : 1 to 1 : 20. Finally, we confirm that 0.05 mg PF543 and 5 mg CBP added to 5 mg PLGA could achieve the best encapsulation efficiency of both of these drugs. Briefly, 5 mg PLGA and 0.05 mg PF543 were dissolved in 0.5 mL dichloromethane (DCM). 50 μL RNase-free water containing 5 mg CBP was added to the above DCM solution. Then the mixture was sonicated at 30% power and pulsed (2 s on/2 s off) for 5 min using a probe sonicator (Scientz Biotechnology, China). 4 mL of 1% F68 solution was added dropwise to a continuously vortexed tube with the above primary emulsion and sonicated with the same setting to form a double emulsion. A rotary evaporator (Yarong, China) was used to remove DCM from C/PNPs under reduced pressure. The C/PNPs were collected after centrifuging at 15 000 rpm for 20 min at 4 °C and washed twice with double-distilled water to remove unentrapped drugs. The constructed C/PNPs were screened by testing both the morphological features and encapsulation efficiency. Compliant C/PNPs were lyophilized for long-term storage. Based on our previous study,[19] 100 μg of Coumarin-6 or DiR was added to 5 mg PLGA and the preparation was the same as the construction of C/PNPs. The size and ζ potential of C/PNPs were tested with a Zetasizer (Nano ZS, Malvern, U.K.). The morphology of C/PNPs was determined using a transmission electron microscope (FEI Co., Hillsboro, OR). The CBP or PF543 encapsulated in C/PNPs was measured by high-performance liquid chromatography (HPLC, Agilent 1200). The encapsulation efficiency (EE%) was calculated as follows: EE% = (CBP or PF543 entrapped in NPs/CBP or PF543 initially added) × 100%.

2.4. Drug release of C/PNPs

C/PNPs were suspended in PBS and incubated at 37 °C under constant rotation. At different time points, an ultrafiltration tube (Millipore, MWCO = 100 kDa) was used to ultra-filter these suspensions. Dialysis tubes (MWCO = 3.5 kDa) containing 1 mL of sample were immersed into 19 mL of PBS with 1 M sodium salicylate along with shaking at 100 rpm. At indicated time points, 200 μL aliquots from the flask were removed for the concentration detection of CBP or PF543 by HPLC and 200 μL of fresh PBS containing sodium salicylate were added back.

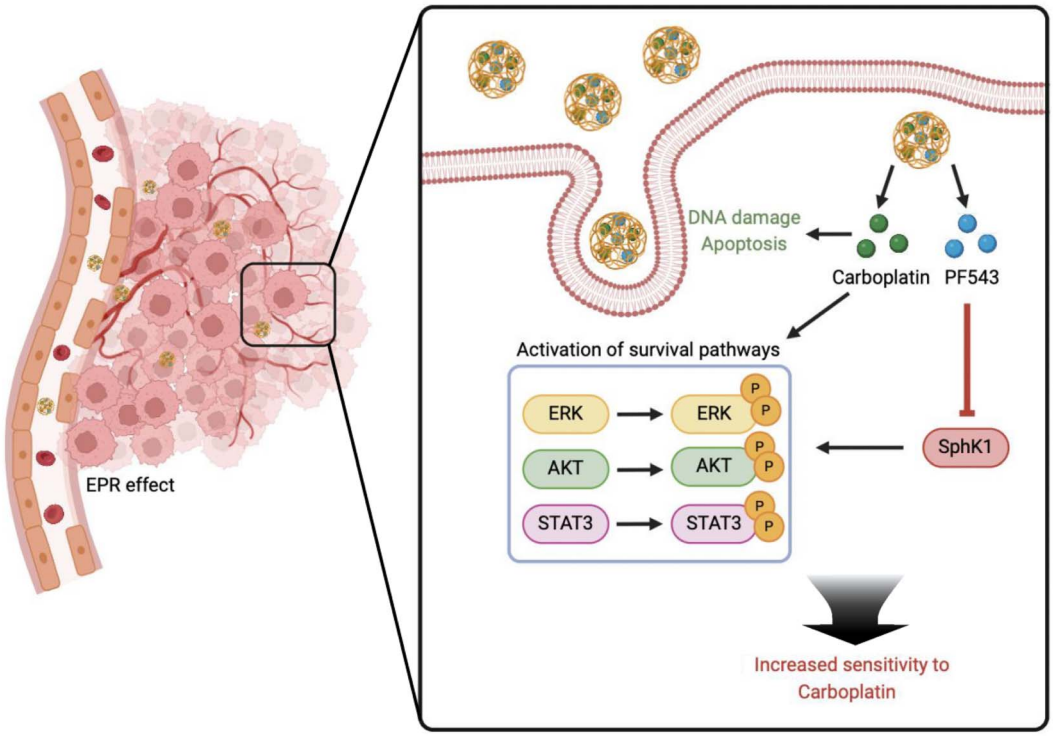

Scheme 1 Nanoparticle co-delivery of carboplatin and PF543, a specific SphK1 inhibitor, restores platinum sensitivity in ovarian cancer by inhibiting the platinum-induced activation of pro-survival pathways, such as ERK, AKT and STAT3 signaling.

2.5. *In vitro* cellular uptake

To make the nanoparticles visible, Coumarin-6-loaded nanoparticles (Coumarin-6-NPs) were formulated. SKOV3 cells seeded in six-well plates (5×10^5 cells per well) were cultured with free Coumarin-6 or Coumarin-6-NPs at a Coumarin-6 concentration of 2 μg mL^{-1}. After 4, 8, 12, and 24 h, the cells that ingested the fluorescent dye were observed under a fluorescence microscope after DAPI staining.

2.6. Cytotoxicity assay

SKOV3 cells were seeded at 3000 cells per well in 96-well plates and cultured overnight. Free drugs or drug-loaded nanoparticles were added at an indicated CBP concentration and a fixed PF543 concentration (100 nM). After 48 h, cell viability was detected with a Cell Counting Kit-8 (CK04; Dojindo, Kumamoto, Japan) according to the manufacturer's protocol. The absorbance was measured with a microplate reader (Thermo Scientific, MA, USA) at a wavelength of 450 nm. To estimate the biocompatibility of the PLGA NPs, cells were incubated with the PLGA NPs for 24 h, 48 h and 72 h, and then the cell viability was assessed by the same method.

2.7. Cell apoptosis analysis

SKOV3 cells were treated with NPs, free CBP, CNPs, free PF543, PNPs, free CBP + PF543 or C/PNPs at a fixed CBP dose (5 μM) and PF543 dose (100 nM) for 48 h. The cells were harvested and double-stained using an Annexin V-FITC Apoptosis Detection Kit (559763; BD-Pharmingen, San Diego, CA, USA) following the manufacturer's instructions. The apoptosis rates of cells were analyzed using FlowJo software (Version X; TreeStar, Ashland, OR, USA).

2.8. Western blot

Western blotting was performed as previously described.[25] Briefly, RIPA lysis buffer (P0013; Beyotime, Nantong, Jiangsu, China) supplemented with protease inhibitor cocktail (ST506; Beyotime, Nantong, Jiangsu, China) was used to split SKOV3 cells or tumor tissue after indicated treatments. The BCA reagent (P0012; Beyotime, Nantong, Jiangsu, China) was used to determine the concentration of proteins. The protein was added into 10% standard SDS gel for electrophoresis until proteins of different molecular weights were separated. Then the protein was transferred to a PVDF membrane (R1CB73920; Millipore, Billerica, MA, USA). The PVDF membrane with protein on it was blocked using 5% bovine serum albumin for 1 h at room temperature. Then the membrane was probed with the indicated primary antibodies at 4 °C overnight. TBST was used to wash the PVDF membrane. After washing, the membrane was incubated with indicated secondary antibodies for 1 h at room temperature. Indicated proteins on the membrane were visualized with an Odyssey Film Scanner.

2.9. *In vivo* imaging and biodistribution studies

Female BALB/c nude mice (4 to 6 weeks old, 18–22 g) were obtained from the Chinese Academy of Sciences and kept in a room at 22 °C with 55% relative humidity and controlled light

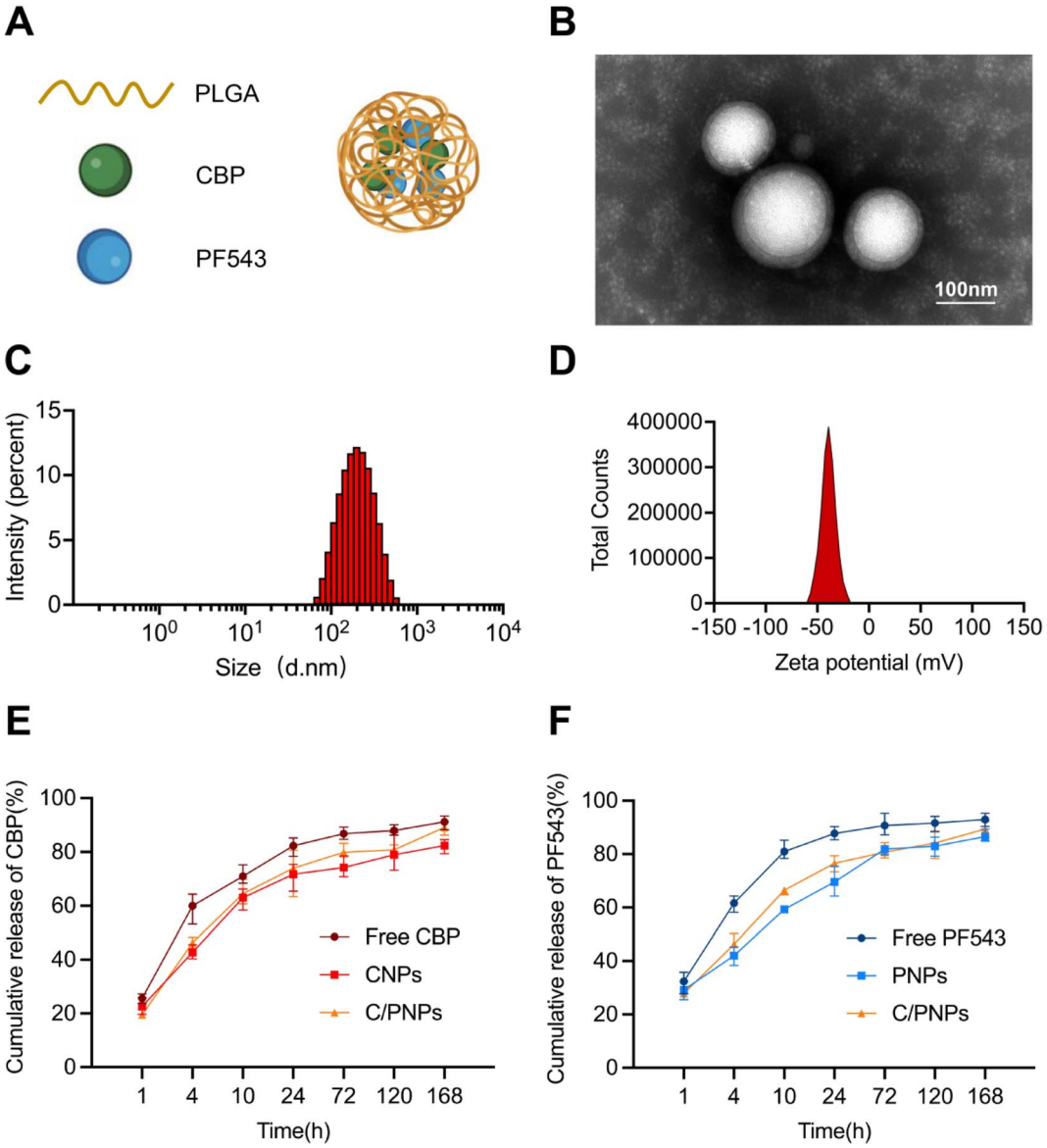

Fig. 1 Preparation and characterization of C/PNPs. (A) Schematic description of the C/PNPs carrying CBP and PF543 in the core. (B) TEM image of C/PNPs. Scale bar, 100 nm. Size distribution (C) and ζ potential (D) of C/PNPs. Data are mean ± SD ($n = 3$). (E) Release profiles of free CBP, CNPs, and C/PNPs. Data are mean ± SD ($n = 3$). (F) Release profiles of free PF543, PNPs, and C/PNPs. Data are mean ± SD ($n = 3$).

for one week of acclimation before use in the experiments. All the animal experimental procedures were conducted with the approval of the Animal Experimentation Ethics Committee of Shanghai Jiao Tong University. The subcutaneous xenograft model was established by injecting SKOV3 cells (2×10^6 cells) into the right foreleg of mice. Whole body fluorescence images were obtained using an *in vivo* imaging system (Xenogen, USA) (Ex/Em: 748/780) at 2, 8, 24 h, and 48 h after injection of free DiR or DiR-NPs at a DiR concentration of 0.4 mg kg^{-1}. Tumors and major organs were collected for *ex vivo* imaging.

2.10. *In vivo* antitumor study

The subcutaneous xenograft model was established using the method mentioned above. The mice were randomly divided into 8 groups ($n = 5$) and injected with PBS, NPs, CBP, CNPs, PF543, PNPs, CBP + PF543 or C/PNPs at a fixed CBP dose (2 mg kg^{-1}) and PF543 dose (0.05 mg kg^{-1}) *via* the tail vein every 2 days. The tumor volume and the body weight of the mice were monitored every 2 days. The tumor volume was calculated as follows: volume = (width^2 × length)/2. Three days after the last injection, the mice were sacrificed after blood collection. The tumors were collected for TUNEL assay and the major organs were collected for H&E staining. The white blood cell (WBC) count, alanine aminotransferase (ALT), and aspartate transaminase (AST) were measured to further evaluate the biosafety of PLGA-based formulations. Histological sections of the heart, liver, spleen, lung and kidney were stained with hematoxylin–eosin and observed under a microscope.

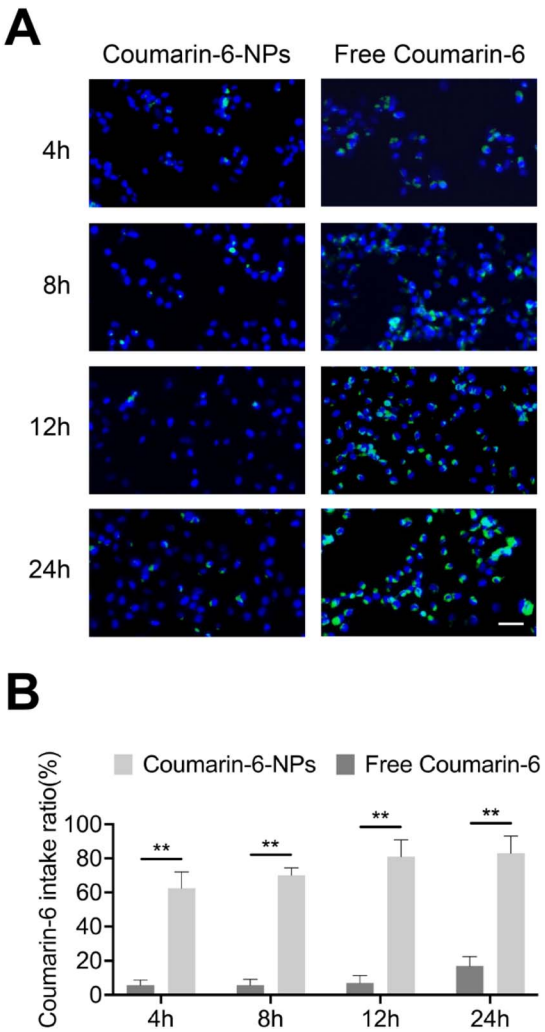

Fig. 2 Cellular uptake of the NPs *in vitro*. (A) Fluorescence microscopy images of SKOV3 cells after 4, 8, 12 and 24 h of incubation with free Coumarin-6 (2 μg mL^{-1}) or Coumarin-6-NPs (2 μg mL^{-1}). Scale bar, 50 μm. The nucleus was stained with DAPI (blue); the drug loaded into the NPs was labeled with Coumarin-6 (green). (B) Quantification of the fluorescence intake ratio of Coumarin-6 in (A). Data are shown as mean ± SD ($n = 3$). **$p < 0.01$.

2.11. Statistical analysis

The experiments were performed in triplicate. Statistical analysis was performed using SPSS software (IBM Corporation, Armonk, NY, USA). The values were presented as mean ± SD and analyzed by a *t*-test ($p < 0.05$ was considered significant).

3 Results and discussion

3.1. Preparation and characterization of C/PNPs

CBP/PF543 co-loaded nanoparticles (C/PNPs) were formulated according to a double-emulsion solvent evaporation method,[26] as shown in Fig. 1A. The CBP-loaded nanoparticles (CNPs) and PF543-loaded nanoparticles (PNPs) were produced by the same method. The transmission electron microscopy (TEM) imaging revealed that C/PNPs possessed a typical spherical shape and good monodispersity with no aggregation (Fig. 1B). Dynamic light scattering (DLS) data showed that the size of Si/PNPs was about 187.9 nm and its ζ potential was about −35.53 mV (Fig. 1C, D and Table S1†). Previous research has indicated that PLGA NPs could efficiently encapsulate chemotherapeutic drugs or genes.[18,19,27] Our studies showed that both CBP and PF543 were encapsulated efficiently in both single agent and dual agent NP formulations. The EE% of CBP and PF543 in C/PNPs was 82.37 ± 0.13% and 89.23 ± 0.03%, respectively (Table S2†).

The release of CBP and PF543 in C/PNPs was next characterized. With respect to both CBP and PF543, a gradual release of approximately 80% occurred within 24 h and the sustained release continued over 168 h (Fig. 1E and F). These data suggested that there was a sequential and slow release of both CBP and PF543 within C/PNPs compared to the rapid release of free CBP and PF543.

3.2. Cellular uptake

The appropriate particle size helps nanoparticles permeate tumor sites and be taken by tumor cells.[28] Coumarin-6 was used to imitate drugs[29] and the cellular uptake of PLGA NPs for the SKOV3 cells was investigated using fluorescence microscopy (Fig. 2A). The uptake of free Coumarin-6 reached a peak at 24 h with an intake ratio of 17.5%. However, the uptake rate of Coumarin-6-NPs obviously enhanced over time, with an intake ratio of 83.4% at 24 h (Fig. 2B). The data suggest that the uptake of drugs was enhanced by PLGA NPs. The appropriate size mainly contributed to the endocytosis of the NPs.[30] In conclusion, PLGA NPs could successfully overcome the obstacle of cellular uptake in drug delivery.

3.3. *In vitro* antitumor effects and alteration of pathways

The dose-dependent cytotoxicity of free CBP, CNPs, free PF543, PNPs, free CBP + PF543, and C/PNPs was evaluated (Fig. 3A). The results showed that a low dose of PF543 (100 nM) itself had nearly no influence on the viability of SKOV3 cells. At each CBP concentration, the cell viability displayed a gradual decrease in the sequence of free CBP, CNPs, free CBP + PF543, and C/PNPs. Compared with free CBP, free CBP + PF543 and C/PNPs exhibited enhanced cell killing effects. Furthermore, the apoptosis rates of SKOV3 cells treated with different formulations were tested (Fig. 3B and C). At a constant CBP concentration of 5 μM, there was a gradual increase in the apoptosis rate exhibited in the following sequence: free PF543 < PNPs < free CBP < CNPs < free PF543 + CBP < C/PNPs. These results indicated that inhibiting SphK1 expression in SKOV3 cells by PF543 could sensitize cancer cells to the CBP treatment. Moreover, the encapsulation of CBP and PF543 by PLGA NPs further enhanced the anti-tumor efficacy.

It has been widely observed that the activation of pro-survival pathways in cancer cells contributes to chemo-resistance and tumor development.[31–33] To identify the alteration of pro-survival pathways induced by CBP, SKOV3 cells were treated with 5 μM CBP. 12 h after treatment, the expressions of phospho-ERK, phospho-AKT and phospho-STAT3 were significantly upregulated (Fig. 3D). The activation of the ERK, AKT and

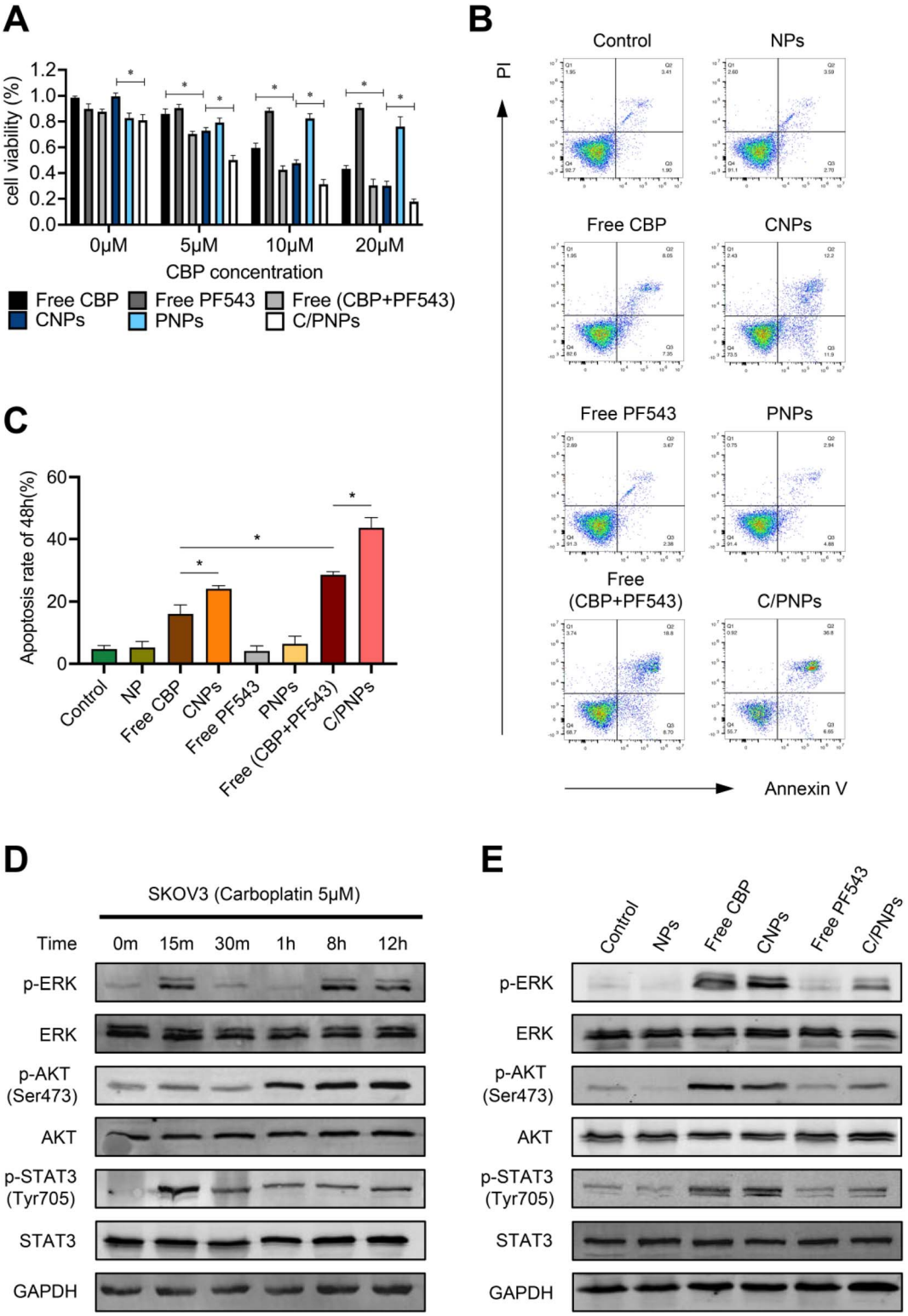

Fig. 3 Cytotoxicity evaluation of C/PNPs. (A) Cell viability of SKOV3 cells when treated with various formulations at indicated CBP concentrations and fixed PF543 concentrations (100 nM) for 48 h. (B) Flow cytometry analysis of SKOV3 cell apoptosis induced by free CBP, free PF543, free (CBP + PF543), CNPs, PNPs or C/PNPs at a CBP concentration of 5 μM and a PF543 concentration of 100 nM for 48 h. (C) Corresponding statistics on the proportion of apoptotic cells. (D) Alteration of the pathways in the SKOV3 cells when treated with 5 μM CBP for indicated times. (E) The effects of C/PNPs on CBP-induced alteration of pathways in the SKOV3 cells, as detected by western blotting. Data are given as mean ± SD ($n = 3$). *$p < 0.05$.

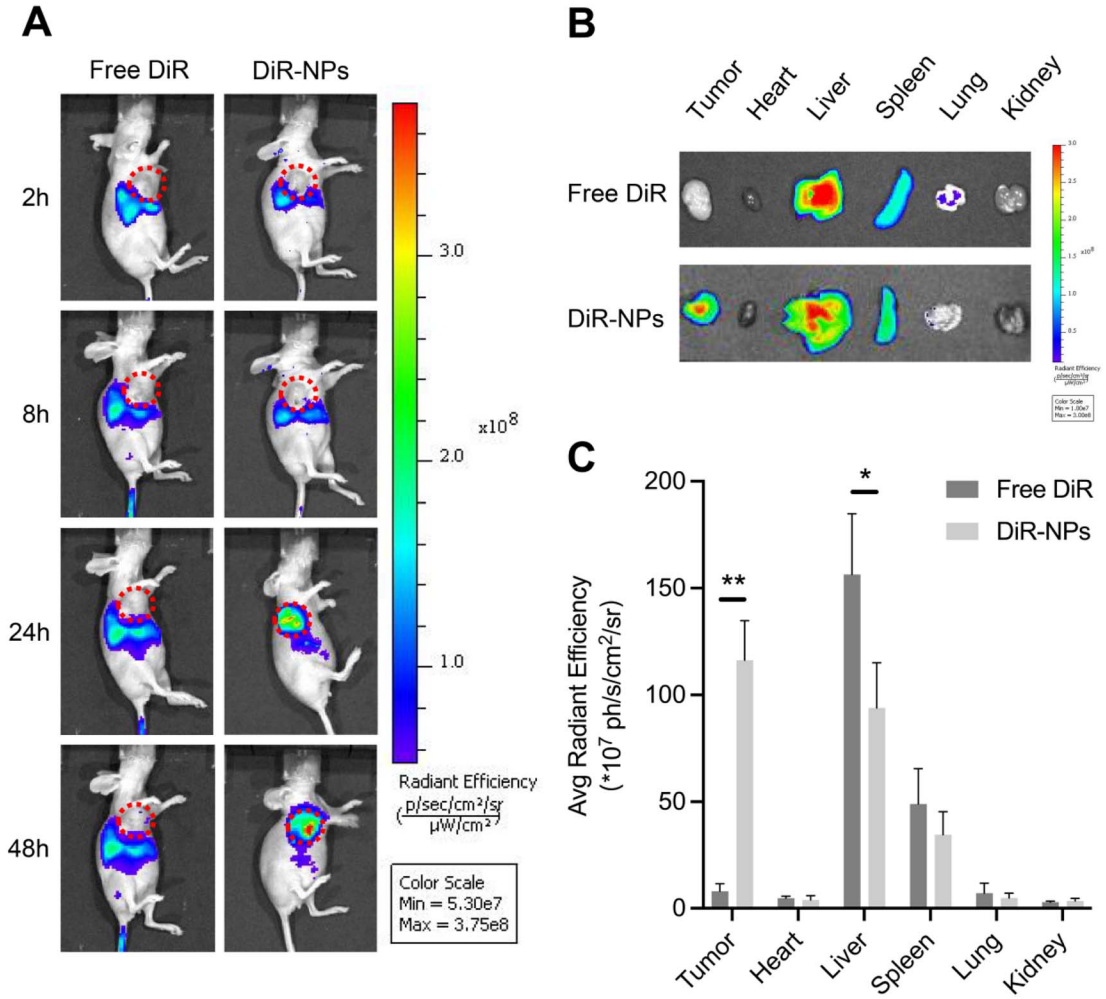

Fig. 4 Biodistribution and pharmacokinetics of NPs. (A) Whole body fluorescence images of SKOV3 subcutaneous xenograft mice at 2, 8, 24, and 48 h after the injection of free DiR or DiR-NPs (at a DiR dose of 0.4 mg kg^{-1}). The tumor area is circled in red. (B) Representative *ex vivo* images of the tumor, heart, liver, spleen, lung, and kidney at 48 h post-injection of free DiR or DiR-NPs. (C) The corresponding average radiation efficiency of resected tumors and major organs. Data are given as mean ± SD ($n = 3$ mice per group). *$p < 0.05$, **$p < 0.01$.

STAT3 pathways was associated with drug resistance in ovarian cancer.[34–36] Therefore, we next explored the changes of the expression of ERK, phospho-ERK, AKT, phospho-AKT, STAT3, and phospho-STAT3 in the SKOV3 cells after incubation with different formulations for 12 h. As shown in Fig. 3E, the ERK, AKT and STAT3 pathways were obviously activated after the treatment of CBP. Nevertheless, the activation of the pro-survival pathways was partially inhibited by PF543 encapsulated in C/PNPs. These data suggested that PF543 in C/PNPs may sensitize SKOV3 cells to CBP partly by inhibiting the CBP-induced activation of pro-survival pathways, including ERK, ATK and STAT3 signaling. However, the exact mechanism of C/PNPs is still far from clear. Other pathways, such as the nuclear factor-κB (NF-κB) pathway and mTOR/S6K1 pathway, are also associated with the platinum resistance of cancer.[37,38] Moreover, NF-κb and mTOR were reported to be regulated by SphK1.[39,40] Therefore, these pathways may also be involved in the restoration of platinum sensitivity in ovarian cancer models induced by C/PNPs. Further in-depth investigations are needed to reveal the novel mechanisms.

3.4. Biodistribution and pharmacokinetics

An effective delivery system needs to accumulate the drug on the tumor site and then improve the efficacy of the drug and reduce the adverse effects on normal organs.[41] We investigated the bio-distribution patterns of PLGA NPs using the SKOV3 subcutaneous xenograft mouse model. DiR was widely used as a tracer in the studies of NPs since the dye can be stably retained in NPs.[42,43] DiR was encapsulated in the PLGA NPs to form DiR-loaded nanoparticles (DiR-NPs) for *in vivo* imaging. As shown in Fig. 4A, no marked fluorescence signal was observed in the tumor site after intravenous injection with free DiR during the whole observation period of 48 h. In contrast, DiR-NPs significantly increased the accumulation of DiR in the tumor site at 24 h probably through the EPR effect.

48 hours after injection, *ex vivo* imaging of primary organs was performed (Fig. 4B). The quantitative estimation of biodistribution by using the average radiation efficiency showed that the content of DiR in both tumor and liver sites of the DiR-NP group was much higher than that of the free DiR group

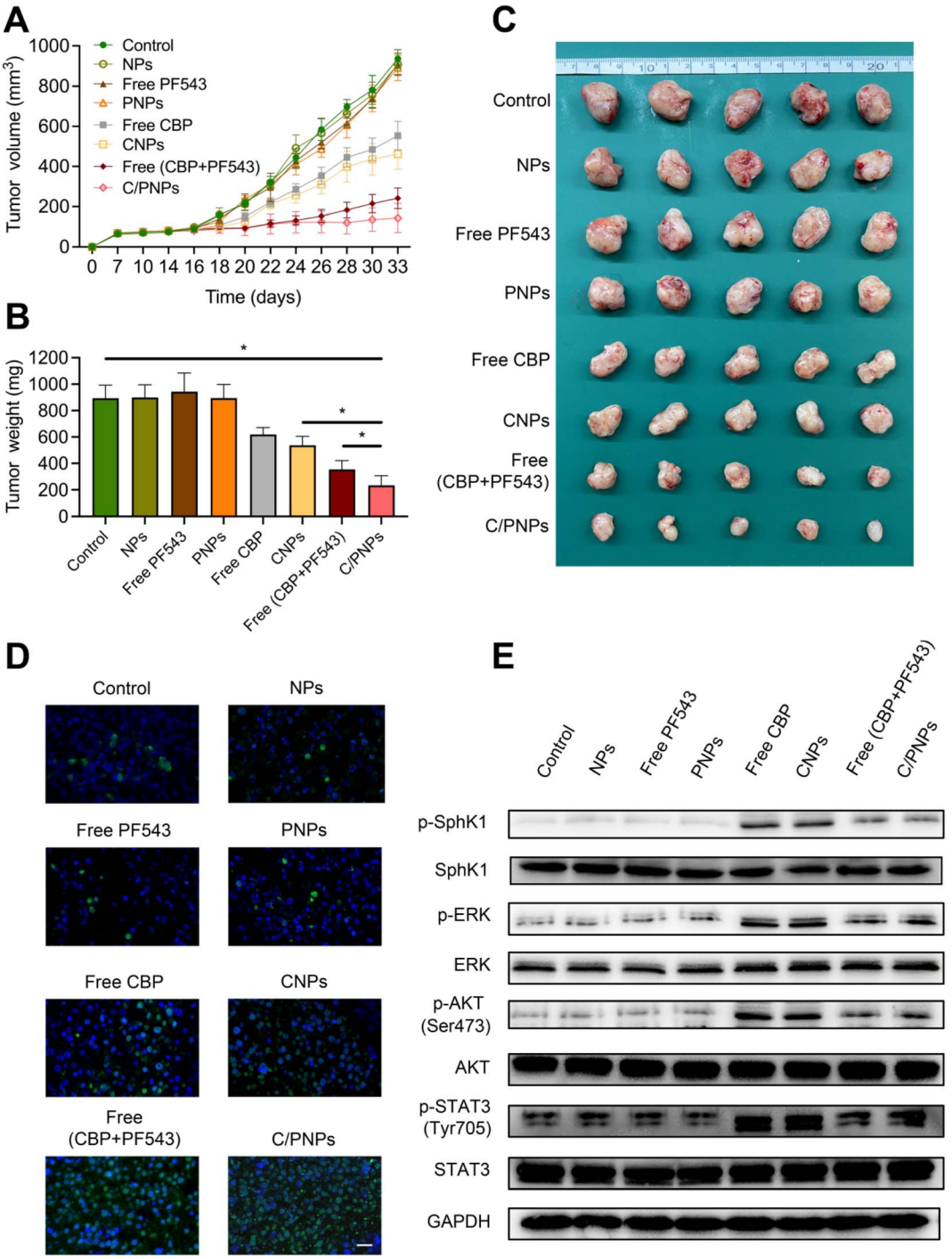

Fig. 5 *In vivo* antitumor effects. (A) Tumor growth profiles of SKOV3 tumor-bearing mice receiving intravenous injections of different formulations every 2 days, for 9 injections, at a fixed CBP dose (2 mg kg^{-1}) and PF543 dose (0.05 mg kg^{-1}). Tumor weight (B) and photographs of the collected tumor tissues (C) on day 33. (D) Representative images of TUNEL assay (scale bar, 50 μm) of tumor tissue. (E) The effects of C/PNPs on CBP-induced alteration of pathways in the tumors, as detected by western blotting. Data are given as mean ± SD ($n = 5$ mice per group). *$p < 0.05$.

(Fig. 4C). However, there was no obvious difference in the content of the dye accumulated in the heart, spleen, lung or kidney. These results were consistent with the well-known fact that PLGA NPs have an effective tumor-targeting effect due to their suitable size and the EPR effect.

3.5. *In vivo* antitumor efficacy

The anticancer efficacy of C/PNPs was investigated in a SKOV3 subcutaneous xenograft mouse model. In order to demonstrate that an optimal anti-tumor effect could be achieved by C/PNPs at a low dose, the total dose of CBP used in mice in this study

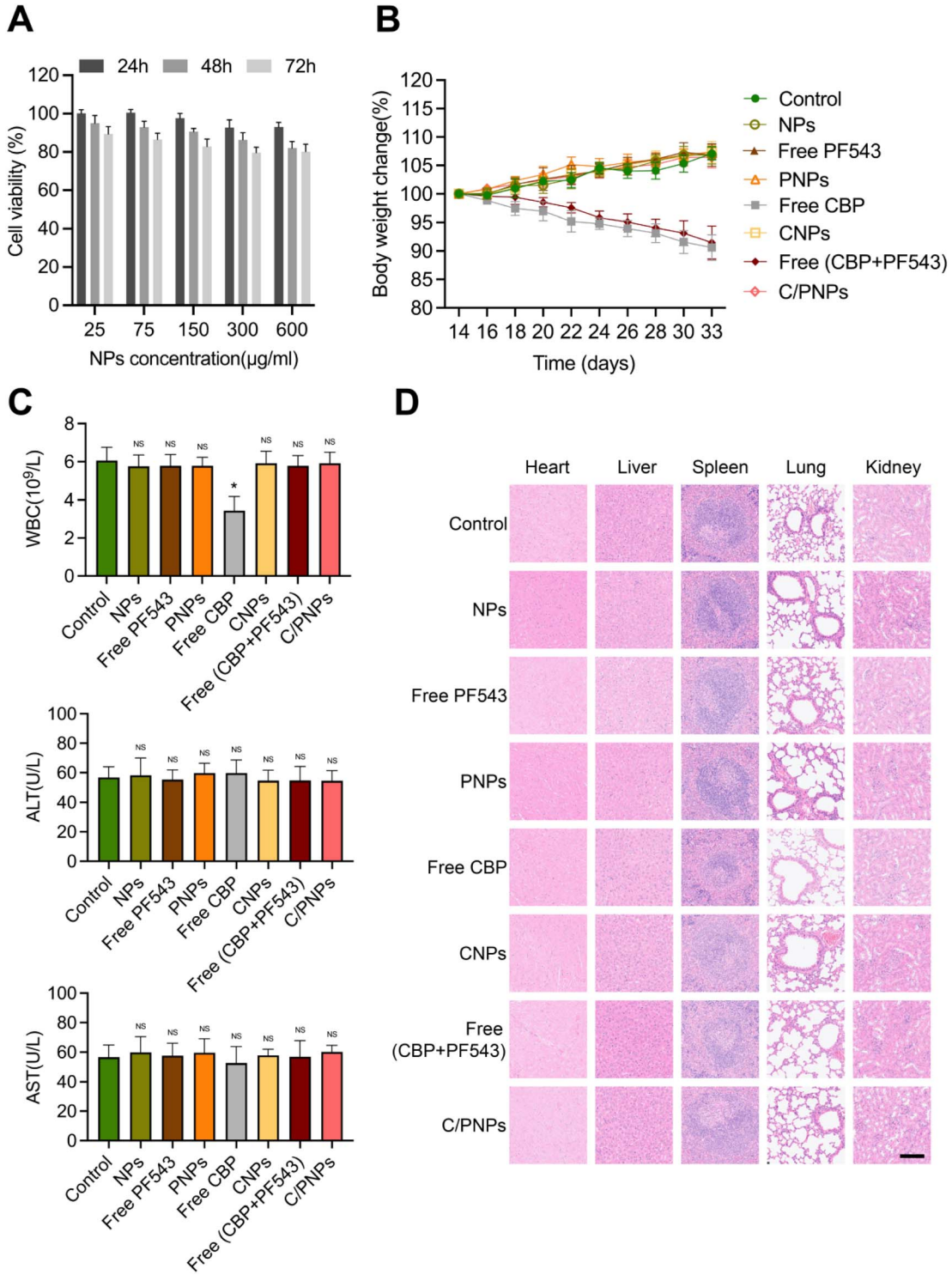

Fig. 6 Biosafety estimation of various formulations. (A) Cytotoxicity of NPs against SKOV3 cells after treatment with different concentrations. (B) Effects of different formulations on the body weight of SKOV3 subcutaneous xenograft mice. (C) Test results of the white blood cell count, plasma ALT, and AST at the end of treatment. (D) Representative H&E staining histological images of major organs from mice receiving different treatments. Scale bar, 100 μm. Data are given as mean ± SD (n = 5 mice per group). *p < 0.05 and NS indicates p > 0.05.

(2 mg kg^{-1} *via* tail-vein injection, for a total of nine injections) was much lower than that of the human clinical equivalent dosage.[44] As shown in Fig. 5A–C, the therapeutic effect of CBP at a dose of 2 mg kg^{-1} was mild. Similarly, the CNP group showed a limited improvement in therapeutic effect. However, the co-delivery of CBP and PF543 resulted in a synergistic effect in inhibiting the growth of tumors, which was further increased by delivering these drugs using PLGA NPs. The tumor volume inhibiting rate was 84.64% for the group receiving C/PNPs, whereas the tumor volume inhibiting rate was 2.94%, 2.65%,

4.73%, 40.76%, 50.63% and 74.16% for the groups receiving NPs, free PF543, PNPs, free CBPs, CNPs and free CBP + PF543, respectively (Fig. 5A), which correlated well with tumor weight changes (Fig. 5B). The tumor weight was 233.54 ± 74.06 mg for the group receiving C/PNPs, whereas the tumor weights were 893.08 ± 100.47, 899.48 ± 96.08, 943.95 ± 104.4, 894.81 ± 103.67, 618.78 ± 52.41, 537.39 ± 67.64 and 354.6 ± 66.54 mg for the groups receiving PBS, NPs, free PF543, PNPs, free CBPs, CNPs and free CBP + PF543, respectively. The apoptosis rates of tumor cells were detected by TUNEL assay (Fig. 5D). Compared with free CBP and CNPs, the apoptosis rate of tumor cells in free CBP + PF543 and C/PNP groups was much higher. As shown in Fig. 5E, the use of CBP or CNPs could activate the phosphorylation of SphK1 and then increase the expression of pro-survival pathways like p-ERK, p-AKT and p-STAT3. Meanwhile the activation of pro-survival signaling pathways could be inhibited by free CBP + PF543 or C/PNPS. These data showed that C/PNPs had a more potent anti-tumor effect compared to single drug loaded NPs or free drugs.

However, the subcutaneous xenograft ovarian cancer mouse model was unable to simulate the development of ovarian cancer in the human body. There are many disadvantages in using this mouse model for evaluating the antitumor efficacy of C/PNPs. In our further study, patient-derived xenografts of ovarian cancer or orthotopic ovarian cancer-bearing mouse models will be used to test the treatment efficacy of NPs.

3.6. *In vitro* and *in vivo* biosafety evaluation

The toxicity of NPs is the major problem in the application of NP pharmaceuticals.[45] We first estimated the cytotoxicity of NPs on a SKOV3 cell. The cell viability remained above 70% at different time points ranging from 24 to 72 h and different concentrations ranging from 25 to 600 μg mL^{-1} (Fig. 6A), which indicated the low cytotoxicity of the PLGA NPs, which is necessary for a drug carrier. Further study was performed to assess the biosafety *in vivo* by evaluating the weight of mice in the different groups mentioned above. Mice treated with PBS, NPs, free PF543, PNPs, free CBP + PF543 and C/PNPs showed negligible body weight changes throughout the whole treatment period, while a significant weight loss was observed in CBP and CNP groups (Fig. 6B). Since myelosuppression and hepatotoxicity are well-known adverse effects in the clinical application of CBP,[46] further study assessed the level of WBCs, ALT and AST. The results showed that mice receiving free CBP exhibited obvious leukopenia rather than mice treated with other different formulations. In contrast, there was no significant difference in the levels of ALT or AST of mice in all groups (Fig. 6C). No pathological changes were found in the slices of the heart, liver, spleen, lung and kidney in all groups (Fig. 6D). These results confirmed the good biocompatibility of C/PNPs. Furthermore, the delivery of CBP by PLGA NPs may alleviate the myelosuppression of CBP to some degree.

4 Conclusions

Overcoming platinum resistance remains a pressing challenge in ovarian cancer therapy. We have developed PLGA NPs capable of co-loading with CBP and the SphK1 inhibitor PF543 to restore platinum sensitivity. Firstly, PLGA NPs mediate highly specific targeted delivery of CBP and PF543 to the tumor tissue by the EPR effect. Secondly, the inhibition of SphK1 by PF543 could restore the platinum sensitivity of ovarian cancer partly by suppressing the CBP-induced activation of multiple pro-survival pathways, key mediators in the sensitivity of tumor cells toward platinum. In addition to PF543, further exploration is needed to explore other means of inhibiting SphK1, such as siRNA, shRNA or CRISPR. It could be envisioned that this nanoplatform can be further used for the co-delivery of platinum drugs with other small molecule anticancer drugs or gene editing tools against SphK1 to achieve a synergistic effect in treating tumors with high expression of SphK1, such as lung cancer, breast cancer, and ovarian cancer. Moreover, as platinum resistance is also present in many other tumors, this dual-drug delivery system may also be effective in the treatment of other platinum insensitive cancers.

Ethical statement

Experiments were carried out in accordance with NIH Guidelines for the Care and Use of Laboratory Animals, with approval from the Animal Experimentation Ethics Committee of Shanghai Jiao Tong University (RA-2019-076) and have adhered to the ARRIVE guidelines. The mice were placed in temperature- and humidity-controlled chambers. The mice were sacrificed under deep anesthesia with sodium pentobarbital (30 mg kg^{-1} i.p.). This study took 46 nude mice (6 for observing the biodistribution patterns of PLGA NPs and 40 for detecting the *in vivo* antitumor efficacy of different formulations).

Data availability

Please contact the corresponding author for all data requests.

Author contributions

WD, LD and NZ: designed the study. CW, QL, WJW and KQS: performed the experiments and analyzed the data. CW, LD and NZ: wrote and revised the manuscript. All authors have read and approved the final manuscript.

Conflicts of interest

The authors declared that there was no conflict of interest.

Acknowledgements

This research was supported by the National Natural Science Foundation of China (NSFC) (Grant No. 81974401 and 81974454), Natural Science Foundation of Science and Technology Commission of Shanghai Municipality (Grant No. 23JC1403000 and 22ZR1438700), Research Promotion Project of Ren Ji Hospital (RJTJ22-ZD-007) and Shanghai Municipal Key Clinical Specialty.

References

1 R. L. Siegel, K. D. Miller, H. E. Fuchs and A. Jemal, Cancer statistics, 2022, *Ca-Cancer J. Clin.*, 2022, **72**(1), 7–33.
2 S. Lheureux, M. Braunstein and A. M. Oza, Epithelial ovarian cancer: Evolution of management in the era of precision medicine, *Ca-Cancer J. Clin.*, 2019, **69**(4), 280–304.
3 E. L. Christie and D. D. L. Bowtell, Acquired chemotherapy resistance in ovarian cancer, *Ann. Oncol.*, 2017, **28**(suppl_8), viii13–viii15.
4 G. C. Jayson, E. C. Kohn, H. C. Kitchener and J. A. Ledermann, Ovarian cancer, *Lancet*, 2014, **384**(9951), 1376–1388.
5 J. J. Marin, R. Al-Abdulla, E. Lozano, O. Briz, L. Bujanda, J. M. Banales, *et al.*, Mechanisms of Resistance to Chemotherapy in Gastric Cancer, *Anti Cancer Agents Med. Chem.*, 2016, **16**(3), 318–334.
6 R. J. Parker, A. Eastman, F. Bostick-Bruton and E. Reed, Acquired cisplatin resistance in human ovarian cancer cells is associated with enhanced repair of cisplatin-DNA lesions and reduced drug accumulation, *J. Clin. Invest.*, 1991, **87**(3), 772–777.
7 M. Binju, M. A. Amaya-Padilla, G. Wan, H. Gunosewoyo, Y. Suryo Rahmanto and Y. Yu, Therapeutic Inducers of Apoptosis in Ovarian Cancer, *Cancers*, 2019, **11**(11), 1786.
8 P. L. Tazzari, A. Cappellini, F. Ricci, C. Evangelisti, V. Papa, T. Grafone, *et al.*, Multidrug resistance-associated protein 1 expression is under the control of the phosphoinositide 3 kinase/Akt signal transduction network in human acute myelogenous leukemia blasts, *Leukemia*, 2007, **21**(3), 427–438.
9 Y. Gao, F. Gao, K. Chen, M. L. Tian and D. L. Zhao, Sphingosine kinase 1 as an anticancer therapeutic target, *Drug Des., Dev. Ther.*, 2015, **9**, 3239–3245.
10 M. J. Pulkoski-Gross and L. M. Obeid, Molecular mechanisms of regulation of sphingosine kinase 1, *Biochim. Biophys. Acta, Mol. Cell Biol. Lipids*, 2018, **1863**(11), 1413–1422.
11 X. Zheng, W. Li, L. Ren, J. Liu, X. Pang, X. Chen, *et al.*, The sphingosine kinase-1/sphingosine-1-phosphate axis in cancer: Potential target for anticancer therapy, *Pharmacol. Ther.*, 2019, **195**, 85–99.
12 O. Cuvillier, Downregulating sphingosine kinase-1 for cancer therapy, *Expert Opin. Ther. Targets*, 2008, **12**(8), 1009–1020.
13 K. Song, L. Dai, X. Long, W. Wang and W. Di, Follicle-stimulating hormone promotes the proliferation of epithelial ovarian cancer cells by activating sphingosine kinase, *Sci. Rep.*, 2020, **10**(1), 13834.
14 J. Liang, M. Nagahashi, E. Y. Kim, K. B. Harikumar, A. Yamada, W. C. Huang, *et al.*, Sphingosine-1-phosphate links persistent STAT3 activation, chronic intestinal inflammation, and development of colitis-associated cancer, *Cancer Cell*, 2013, **23**(1), 107–120.
15 Z. Qin, H. Tong, T. Li, H. Cao, J. Zhu, S. Yin, *et al.*, SPHK1 contributes to cisplatin resistance in bladder cancer cells via the NONO/STAT3 axis, *Int. J. Mol. Med.*, 2021, **48**(5), 204.
16 Y. Ma, X. Xing, R. Kong, C. Cheng, S. Li, X. Yang, *et al.*, SphK1 promotes development of non-small cell lung cancer through activation of STAT3, *Int. J. Mol. Med.*, 2021, **47**(1), 374–386.
17 H. Zhang, Q. Wang, Q. Zhao and W. Di, MiR-124 inhibits the migration and invasion of ovarian cancer cells by targeting SphK1, *J. Ovarian Res.*, 2013, **6**(1), 84.
18 X. Cui, Y. Sun, M. Shen, K. Song, X. Yin, W. Di, *et al.*, Enhanced Chemotherapeutic Efficacy of Paclitaxel Nanoparticles Co-delivered with MicroRNA-7 by Inhibiting Paclitaxel-Induced EGFR/ERK pathway Activation for Ovarian Cancer Therapy, *ACS Appl. Mater. Interfaces*, 2018, **10**(9), 7821–7831.
19 C. Xu, W. Liu, Y. Hu, W. Li and W. Di, Bioinspired tumor-homing nanoplatform for co-delivery of paclitaxel and siRNA-E7 to HPV-related cervical malignancies for synergistic therapy, *Theranostics*, 2020, **10**(7), 3325–3339.
20 D. Ding and Q. Zhu, Recent advances of PLGA micro/nanoparticles for the delivery of biomacromolecular therapeutics, *Mater. Sci. Eng., C*, 2018, **92**, 1041–1060.
21 M. B. Sokol, M. V. Chirkina, N. G. Yabbarov, M. R. Mollaeva, T. A. Podrugina, A. S. Pavlova, *et al.*, Structural Optimization of Platinum Drugs to Improve the Drug-Loading and Antitumor Efficacy of PLGA Nanoparticles, *Pharmaceutics*, 2022, **14**(11), 2333.
22 P. S. Ong, X. Q. Wang, H. S. Lin, S. Y. Chan and P. C. Ho, Synergistic effects of suberoylanilide hydroxamic acid combined with cisplatin causing cell cycle arrest independent apoptosis in platinum-resistant ovarian cancer cells, *Int. J. Oncol.*, 2012, **40**(5), 1705–1713.
23 W. J. Murdoch, E. A. Van Kirk, D. D. Isaak and Y. Shen, Progesterone facilitates cisplatin toxicity in epithelial ovarian cancer cells and xenografts, *Gynecol. Oncol.*, 2008, **110**(2), 251–255.
24 S. Cheng, C. Xu, Y. Jin, Y. Li, C. Zhong, J. Ma, *et al.*, Artificial Mini Dendritic Cells Boost T Cell-Based Immunotherapy for Ovarian Cancer, *Adv. Sci.*, 2020, **7**(7), 1903301.
25 C. Wang, T. Ye, W. Wang, K. Song, J. Zhu, L. Dai, *et al.*, Sphingosine kinase 1 contributes to the metastatic potential of epithelial ovarian cancer to the adipocyte-rich niche, *Exp. Hematol. Oncol.*, 2022, **11**(1), 102.
26 M. Iqbal, N. Zafar, H. Fessi and A. Elaissari, Double emulsion solvent evaporation techniques used for drug encapsulation, *Int. J. Pharm.*, 2015, **496**(2), 173–190.
27 O. Maksimenko, J. Malinovskaya, E. Shipulo, N. Osipova, V. Razzhivina, D. Arantseva, *et al.*, Doxorubicin-loaded PLGA nanoparticles for the chemotherapy of glioblastoma: Towards the pharmaceutical development, *Int. J. Pharm.*, 2019, **572**, 118733.
28 J. L. Perry, K. G. Reuter, J. C. Luft, C. V. Pecot, W. Zamboni and J. M. DeSimone, Mediating Passive Tumor Accumulation through Particle Size, Tumor Type, and Location, *Nano Lett.*, 2017, **17**(5), 2879–2886.

29 S. Pretor, J. Bartels, T. Lorenz, K. Dahl, J. H. Finke, G. Peterat, *et al.*, Cellular uptake of coumarin-6 under microfluidic conditions into HCE-T cells from nanoscale formulations, *Mol. Pharm.*, 2015, **12**(1), 34–45.

30 E. Linnane, S. Haddad, F. Melle, Z. Mei and D. Fairen-Jimenez, The uptake of metal-organic frameworks: a journey into the cell, *Chem. Soc. Rev.*, 2022, **51**(14), 6065–6086.

31 P. R. Singh, E. S. Priya, S. Balakrishnan, R. Arunkumar, G. Sharmila, M. Rajalakshmi, *et al.*, Nimbolide inhibits androgen independent prostate cancer cells survival and proliferation by modulating multiple pro-survival signaling pathways, *Biomed. Pharmacother.*, 2016, **84**, 1623–1634.

32 D. Mehlich, M. Lomiak, A. Sobiborowicz, A. Mazan, D. Dymerska, L. M. Szewczyk, *et al.*, MLK4 regulates DNA damage response and promotes triple-negative breast cancer chemoresistance, *Cell Death Dis.*, 2021, **12**(12), 1111.

33 J. L. Young, X. Hua, H. Somsel, F. Reichart, H. Kessler and J. P. Spatz, Integrin Subtypes and Nanoscale Ligand Presentation Influence Drug Sensitivity in Cancer Cells, *Nano Lett.*, 2020, **20**(2), 1183–1191.

34 X. Zhang, Z. Qi, H. Yin and G. Yang, Interaction between p53 and Ras signaling controls cisplatin resistance via HDAC4- and HIF-1alpha-mediated regulation of apoptosis and autophagy, *Theranostics*, 2019, **9**(4), 1096–1114.

35 D. Parashar, A. Geethadevi, S. Mittal, L. A. McAlarnen, J. George, I. P. Kadamberi, *et al.*, Patient-Derived Ovarian Cancer Spheroids Rely on PI3K-AKT Signaling Addiction for Cancer Stemness and Chemoresistance, *Cancers*, 2022, **14**(4), 958.

36 M. Giordano, A. Decio, C. Battistini, M. Baronio, F. Bianchi, A. Villa, *et al.*, L1CAM promotes ovarian cancer stemness and tumor initiation via FGFR1/SRC/STAT3 signaling, *J. Exp. Clin. Cancer Res.*, 2021, **40**(1), 319.

37 T. Nakano, K. A. Warner, A. E. Oklejas, Z. Zhang, C. Rodriguez-Ramirez, A. G. Shuman, *et al.*, mTOR Inhibition Ablates Cisplatin-Resistant Salivary Gland Cancer Stem Cells, *J. Dent. Res.*, 2021, **100**(4), 377–386.

38 V. Brabec and J. Kasparkova, Modifications of DNA by platinum complexes. Relation to resistance of tumors to platinum antitumor drugs, *Drug Resistance Updates*, 2005, **8**(3), 131–146.

39 J. Xie, T. Zhang, P. Li, D. Wang, T. Liu and S. Xu, Dihydromyricetin Attenuates Cerebral Ischemia Reperfusion Injury by Inhibiting SPHK1/mTOR Signaling and Targeting Ferroptosis, *Drug Des., Dev. Ther.*, 2022, **16**, 3071–3085.

40 M. Nagahashi, N. C. Hait, M. Maceyka, D. Avni, K. Takabe, S. Milstien, *et al.*, Sphingosine-1-phosphate in chronic intestinal inflammation and cancer, *Adv. Biol. Regul.*, 2014, **54**, 112–120.

41 R. Li, Y. He, S. Zhang, J. Qin and J. Wang, Cell membrane-based nanoparticles: a new biomimetic platform for tumor diagnosis and treatment, *Acta Pharm. Sin. B*, 2018, **8**(1), 14–22.

42 J. Wang, F. Guo, M. Yu, L. Liu, F. Tan, R. Yan, *et al.*, Rapamycin/DiR loaded lipid-polyaniline nanoparticles for dual-modal imaging guided enhanced photothermal and antiangiogenic combination therapy, *J. Controlled Release*, 2016, **237**, 23–34.

43 B. Luo, H. Zhang, X. Liu, R. Rao, Y. Wu and W. Liu, Novel DiR and SPIO nanoparticles embedded PEG-PLGA nanobubbles as a multimodalimaging contrast agent, *Bio-Med. Mater. Eng.*, 2015, **26**(suppl 1), S911–S916.

44 D. K. Armstrong, R. D. Alvarez, J. N. Bakkum-Gamez, L. Barroilhet, K. Behbakht, A. Berchuck, *et al.*, Ovarian Cancer, Version 2.2020, NCCN Clinical Practice Guidelines in Oncology, *J. Natl. Compr. Cancer Network*, 2021, **19**(2), 191–226.

45 A. Zielinska, F. Carreiro, A. M. Oliveira, A. Neves, B. Pires, D. N. Venkatesh, *et al.*, Polymeric Nanoparticles: Production, Characterization, Toxicology and Ecotoxicology, *Molecules*, 2020, **25**(16), 3731.

46 R. Oun, Y. E. Moussa and N. J. Wheate, The side effects of platinum-based chemotherapy drugs: a review for chemists, *Dalton Trans.*, 2018, **47**(19), 6645–6653.